

1

2

3

4 **TMEM55A-mediated PI5P signaling regulates α -cell actin**
5 **depolymerization and glucagon secretion**

6 Xiong Liu^{1, 2}, Theodore dos Santos^{1, 2}, Aliya F. Spigelman^{1, 2}, Shawn Duckett^{1, 2}, Nancy
7 Smith^{1, 2}, Kunimasa Suzuki^{1, 2}, Patrick E. MacDonald^{1, 2*}

8 ¹Department of Pharmacology, University of Alberta, Edmonton, AB T6G 2E1, Canada.

9 ²Alberta Diabetes Institute, University of Alberta, Edmonton, T6G 2E1, Canada.

10

11

12

13

14

15

16 *Correspondence:

17 Patrick E. MacDonald

18 Alberta Diabetes Institute

19 LKS Centre, Rm. 6-126

20 Edmonton, AB

21 Canada, T6G2R3

22 (pmacdonald@ualberta.ca)

23 **Abstract**

24 Diabetes is associated with the dysfunction of glucagon-producing pancreatic islet α -cells,
25 although the underlying mechanisms regulating glucagon secretion and α -cell dysfunction
26 remain unclear. While insulin secretion from pancreatic β -cells has long been known to be
27 partly controlled by intracellular phospholipid signaling, very little is known about the role
28 of phospholipids in glucagon secretion. Here we show that TMEM55A, a lipid phosphatase
29 that dephosphorylates phosphatidylinositol-4,5-bisphosphate (PIP2) to
30 phosphatidylinositol-5-phosphate (PI5P), regulates α -cell exocytosis and glucagon
31 secretion. TMEM55A knockdown in both human and mouse α -cells reduces exocytosis at
32 low glucose, and this is rescued by the direct reintroduction of PI5P. This does not occur
33 through an effect on Ca^{2+} channel activity, but through a re-modelling of cortical F-actin
34 dependent upon TMEM55A lipid phosphatase activity which occurs in response to
35 oxidative stress. In summary, we reveal a novel pathway by which TMEM55A regulates
36 α -cell exocytosis by manipulating intracellular PI5P level and the F-actin network.

37 **Introduction**

38 Glucagon is secreted by α -cells of the pancreatic islets of Langerhans to stimulate
39 glycogenolysis and gluconeogenesis, thereby increasing blood glucose [1]. In diabetes,
40 hypersecretion of glucagon can contribute to postprandial hyperglycemia while an
41 insufficient glucagon response to falling blood glucose levels can lead to hypoglycemia [1].
42 Both intrinsic and paracrine mechanisms control glucagon secretion, however in contrast
43 to the exploration of detailed molecular mechanisms for insulin secretion from β -cells, the
44 mechanisms regulating α -cell activity and glucagon secretion remain largely unclear and
45 debatable [2]. Extrinsically, glucagon secretion is regulated by paracrine factors, such as
46 insulin [3], somatostatin [4], adrenaline [5], and GIP [6]. Intrinsically, α -cell membrane
47 depolarization initiates the opening of voltage-gated Na^+ and P/Q-type Ca^{2+} channels, and
48 a local increase of cytoplasmic Ca^{2+} which triggers the exocytosis of glucagon granules [1].
49 The access of those granules to the plasma membrane is also regulated by the cortical
50 cytoskeleton [7]. Cortical F-actin is reported to act as a barrier to prevent access of insulin
51 granules to the plasma membrane [8, 9], while also providing a path for insulin granule
52 trafficking [10]. In contrast, studies on the relationship between cortical F-actin and
53 glucagon granules in α -cells are sparse [11-13] and the up- or downstream regulatory
54 pathway(s) remains poorly understood.

55 TMEM55A (encoded by the *PIP4P2* gene) was first identified as a phosphatase that
56 catalyzes the hydrolysis of phosphatidylinositol-4,5-bisphosphate (PIP2) to
57 phosphatidylinositol-5-phosphate (PI5P), with no enzymatic activity on other
58 phosphoinositides [14]. It is expressed throughout the body, including in the pancreas [14].
59 Our published pancreas patch-seq data indicated that *PIP4P2* expression is positively
60 correlated with α cell glucagon exocytosis, while negatively correlated with β cell insulin
61 exocytosis [15]. We therefore explored whether and how TMEM55A regulates exocytosis
62 in these cells. In the present study, we examined the role of TMEM55A in human and
63 mouse primary α -cells, and the α TC1-9 cell line. We found that TMEM55A positively
64 regulates α -cell exocytosis, by increasing intracellular PI5P levels to promote F-actin
65 depolymerization via inhibition of the small G-protein RhoA. Oxidative stress acts
66 upstream of TMEM55A/PI5P/F-actin axis, resulting in increased glucagon exocytosis and
67 glucagon hypersecretion.

68 **Results**

69 **Expression of *PIP4P2*, encoding TMEM55A, regulates α -cell function**

70 Our previous correlated electrophysiological and single-cell RNA-seq (patch-seq)
71 studies of α -cells from human donors identified hundreds of transcripts correlated with α -
72 cell function [15]. However, potential causative roles for most of these remain to be
73 elucidated. Mining this data, a lipid phosphatase, TMEM55A (encoded by *PIP4P2*), stood
74 out since it appeared to associate with single-cell function in α -cells. We confirmed the
75 expression of TMEM55A in human α - and β -cells by immunostaining in biopsies from
76 donors with and without T2D (Fig. 1A). Upon analysis of a large patch-seq dataset at
77 www.humanislets.com [16], we found that the expression of *PIP4P2* is positively
78 correlated with the α -cell size, exocytosis, Ca^{2+} currents and Na^+ currents (Fig. 1B), while

79 it does not correlate with most β -cell electrophysiological properties (Fig. 1C). We further
80 compared the correlations in α -cells from donors with or without T2D (ND vs T2D) at 1
81 mM glucose and 5 mM glucose, and found that *PIP4P2* demonstrates a loss of correlation
82 (or even opposite correlation) with α -cell electrophysiology parameters in T2D (Fig. 1D,
83 E), indicating the function of TMEM55A might be dysregulated.

84 To better characterize the role of TMEM55A in islets, *PIP4P2* was knocked down by
85 RNA interference (RNAi) in isolated human islet cells. Knockdown was confirmed at both
86 mRNA (86% reduction) and protein (57% reduction) levels (Fig. 2A, B), and by single-
87 cell immunofluorescence (Fig. 2C and Fig. S1A). Here we did not find any differences in
88 the α -cell size or depolarization-induced Ca^{2+} entry upon the knockdown of *PIP4P2* but
89 found that the α -cell exocytotic response (at 1 mM glucose) was dramatically decreased
90 (Fig. 2D, E), consistent with the correlation analysis above. In β -cells, we found little effect
91 following *PIP4P2* knockdown (Fig. S1 B, C). Since this single-cell exocytosis
92 measurement can inform about mechanistic underpinnings of α -cell function, but does not
93 measure secretion directly, we assessed glucagon secretion stimulated by KCl, low glucose
94 (1 mM), and glucose-dependent insulinotropic polypeptide (GIP, 100 nM) with the amino
95 acid alanine (10 mM) following *PIP4P2* knockdown. Consistently, we found that glucagon
96 secretion from the si-*PIP4P2* transfection group was significantly reduced upon KCl or
97 GIP and alanine stimulation compared with controls (Fig. 2F). These data together suggest
98 the involvement of TMEM55A in the regulation of glucagon secretion.

99 We also measured voltage-dependent Na^+ and Ca^{2+} currents. The si-*PIP4P2*
100 transfected α -cells showed decreased Na^+ currents. However, we did not detect any
101 significant changes in the Ca^{2+} currents (Fig. 2G, H). Consistent with the little effect on β -
102 cell exocytotic response, no differences on the Na^+ or Ca^{2+} currents were found upon
103 *PIP4P2* knockdown in β -cells (Fig. S1 D, E). Since the intracellular Ca^{2+} inhibits voltage-
104 dependent Ca^{2+} channels, we also used Ba^{2+} as a charge carrier and included the Na^+
105 channel inhibitor tetrodotoxin (0.5 μM) in the bath to more closely interrogate Ca^{2+} channel
106 activity. We still found no significant effect of *PIP4P2* knockdown on the Ca^{2+} channel-
107 mediated currents (Fig. 2I), indicating that reduced Ca^{2+} channel activity is not responsible
108 for the decreased α -cell exocytosis we observed above. Indeed, upon infusion of 200 nM
109 free Ca^{2+} into the cell interior, exocytosis from the si-*PIP4P2* transfected α -cells was still
110 lower than controls (Fig. 2J).

111 **A role for PIP2 and PI5P regulating α -cell exocytosis**

112 TMEM55A was initially identified as a phosphatase that dephosphorylates PIP2 to
113 PI5P [14]. As a signaling phospholipid, PIP2 plays critical roles in exocytosis [17, 18],
114 while the physiological relevance of PI5P to exocytosis has never been explored. We
115 therefore examined whether PIP2 or PI5P can regulate α -cell exocytosis. The intracellular
116 dialysis of 1 μM diC₈ PIP2 or PI5P, a water-soluble dioctanoyl analog, increased and
117 decreased human α -cell exocytosis, respectively (Fig. 3 A, B), directionally consistent with
118 what we would expect based on our TMEM55A knockdown studies. Indeed, PI5P infusion
119 rescued the reduced exocytosis in si-*PIP4P2* transfected cells to levels comparable with

120 the controls (Fig. 3C). Similar experiments could also be reproduced using mouse α -cells
121 (Fig. 3 D, E). To better illustrate the role of PIP2 and PI5P on glucagon secretion, we treated
122 mouse islets with 1 μ M PIP2 or PI5P (which are membrane permeable [19, 20]) overnight
123 and found that PIP2 has no obvious effect, while PI5P-treated islets demonstrate increased
124 glucagon secretion (Fig. 3F). This suggests that the decreased glucagon secretion caused
125 by *PIP4P2* knockdown might be due to the decreased intracellular PI5P level, rather than
126 increased PIP2. Of note, neither PIP2 nor PI5P affects glucagon content (Fig. 3G), which
127 is consistent with our knockdown study (Fig. 2F).

128 **Phosphatase activity of TMEM55A**

129 It has been suggested that TMEM55A does not, in fact, have lipid phosphatase activity
130 [21]. To investigate this, and to confirm whether TMEM55A lipid phosphatase activity is
131 involved in the regulation of α -cell function, we generated a wild-type GFP-tagged human
132 TMEM55A (GFP-TMEM55A) and “phosphatase dead” mutant (GFP-TMEM55A C107S).
133 Interestingly, human embryonic kidney (HEK) cells expressing GFP-TMEM55A
134 demonstrated a more round-shape, compared with cells expressing GFP or GFP-
135 TMEM55A C107S (Fig. S2 A, B), suggesting some activity of the WT enzyme influencing
136 cell morphology. Moreover, we detected a large hydrolysis of PIP2 by GFP-TMEM55A,
137 compared with GFP or GFP-TMEM55A C107S, which is even more robust compared with
138 the positive control, the phosphatase enzyme SHIP2 (Fig. 4A). Since PI5P was reported as
139 an oxidative stress-induced second messenger and it is increased in response to hydrogen
140 peroxide (H_2O_2) in diverse cell lines [22], we examined whether TMEM55A activity could
141 be modulated by cellular redox. Here we found that under reducing condition with 1 mM
142 DTT, TMEM55A lipid phosphatase activity is inhibited while subsequent incubation with
143 an oxidizer, 1 mM H_2O_2 activates the enzyme (Fig. 4B).

144 Next, we tested the H_2O_2 sensitivity of TMEM55A *in situ*. Because there is no reliable
145 PI5P sensor, we overexpressed GFP-TMEM55A and PIP2 probe, mCherry-PH-PLC [23]
146 at the same time. Then, we monitored the dynamic PIP2 changes following treatment with
147 1 mM H_2O_2 using live cell imaging. As reported before [24], external application of H_2O_2
148 induced PIP2 hydrolysis. Interestingly, while treatment with H_2O_2 activated PIP2
149 hydrolysis in cells expressing wild-type GFP-TMEM55A, this effect was lost in cells
150 expressing GFP-TMEM55A C107S (Fig. 4C and supplementary video 1-3), indicating that
151 H_2O_2 induced PIP2 hydrolysis depends on the phosphatase activity of TMEM55A.

152 We then knocked down native TMEM55A in α TC1-9 cells. Like in primary α -cells,
153 knocking down TMEM55A decreased glucagon secretion from α TC1-9 cells (Fig. 4D).
154 When we overexpressed GFP-TMEM55A and GFP-TMEM55A C107S, we found that
155 only the wild-type GFP-TMEM55A showed a partially recovered glucagon secretion
156 following TMEM55A knockdown (Fig. 4E). This indicates that TMEM55A control of
157 glucagon secretion depends on its phosphatase activity. Moreover, the product of
158 TMEM55A, PI5P significantly increases glucagon secretion in α TC1-9 cells (Fig. 4F).
159 Taken together, these data suggest that the regulation of TMEM55A on glucagon secretion
160 depends on its lipid phosphatase activity.

161 **RhoA is the downstream signaling molecule of PI5P**

162 PI5P is the least characterized phosphoinositide and its functions remain elusive [25]. It
163 was reported that PI5P might regulate actin dynamics in cell migration [26], and
164 intracellular or extracellular application of PI5P in different cell lines causes F-actin stress
165 fiber breakdown via activation of Rac1 [20, 27]. To address the downstream signaling effect
166 of PI5P in α -cells, we monitored the levels of active Rac1 together with two other major
167 GTPases, Cdc42 and RhoA in α TC1-9 cells following treatment with PI5P. We found that
168 PI5P leads to strong inactivation of RhoA, with no obvious effects on Rac1 or Cdc42 (Fig.
169 5A). Although this contradicts observations in mouse embryonic fibroblast (MEF) cell
170 lines [20], it is in line with the role of RhoA identified in α -cells [12]. Similar experiments
171 could also be reproduced in human islets (Fig. 5B). Expression of GFP-TMEM55A in
172 α TC1-9 cells also resulted in the inactivation of RhoA, while GFP or GFP-TMEM55A
173 C107S had no effect (Fig. 5C). These observations suggested that RhoA is a downstream
174 effector of PI5P and TMEM55A in α -cells.

175 **PI5P regulates α -cell F-actin remodeling**

176 F-actin depolymerization is mainly governed by Rho-family small GTPases [28]. After
177 validation that RhoA is downstream of TMEM55A in α -cells, we wanted to visualize
178 whether PI5P could disrupt the F-actin in α -cells to enhance glucagon secretion. We first
179 confirmed the relationship between F-actin and α -cell exocytosis. Human α -cells treated
180 with 10 μ M latrunculin B or jasplakinolide for 1 h to disrupt and enhance actin
181 polymerization, demonstrated increased and decreased exocytotic responses, respectively,
182 directionally consistent with the effects of TMEM55A and PI5P (Fig. 6A). Then we
183 examined the distribution of F-actin by phalloidin staining using confocal microscopy
184 following PI5P treatment. Consistent with previous studies on MEF and HeLa cell lines
185 [20, 27], PI5P significantly decreased the F-actin intensity in dispersed human and mouse
186 primary α -cells (Fig. 6A, B), in whole islets (Fig. 6C, D), and in α TC1-9 cells (Fig. 6E).
187 Using live-imaging of F-tractin-mCherry, a probe for monitoring global F-actin [29], we
188 found that PI5P disrupted F-actin in a time-dependent manner (Fig. 6F and supplementary
189 video 4-5). Since TMEM55A increases intracellular PI5P, we overexpressed GFP-
190 TMEM55A in α TC1-9 cells and found that α TC1-9 cells overexpressing GFP-TMEM55A
191 demonstrated a low intensity of F-actin compared with cells expressing GFP-TMEM55A
192 C107S or GFP alone (Fig. 6G). Conversely, when we knocked down *PIP4P2* in human α -
193 cells, we detected a significant increase of F-actin (Fig. 6 H), which explains the decreased
194 exocytosis in our functional studies (Fig. 2E). Taken together, these data strongly indicated
195 the involvement of TMEM55A and PI5P in F-actin depolymerization.

196

197 Discussion

198 While T2D results from a complex interplay between insulin resistance and insulin
199 secretion [30, 31] and T1D results from insulin insufficiency due to autoimmune
200 destruction of β -cells [32], both forms of diabetes are associated with disrupted glucagon
201 secretion from islet α -cells [33]. However, the underlying molecular mechanisms that
202 regulate glucagon secretion in α -cells remain unclear. Here we identified TMEM55A as a
203 correlate of α -cell function through bioinformatic analysis of single-cell function and
204 transcript expression. Combined with mechanistic studies on human and mouse primary α -
205 cells and α TC1-9 cell lines, we describe a glucagon regulation mechanism by TMEM55A
206 and PI5P-mediated F-actin depolymerization. We further provide evidence that oxidative
207 stress can modulate TMEM55A activity, and that RhoA acts as a downstream effector of
208 this lipid phosphatase, which is summarized in Fig. 7.

209 TMEM55A was initially identified, along with TMEM55B, as an enzyme that catalyzes
210 PIP2 to PI5P [14]. However, its phosphatase activity has been challenged by recent reports
211 [21, 34], which found that neither recombinant TMEM55A nor TMEM55B catalytic
212 domain demonstrates any detectable phosphatase activity when expressed in *E.coli*. We
213 assumed that the lack of activity could be due to the lack of transmembrane or post-
214 translational modifications [35, 36]. We therefore expressed full-length TMEM55A in
215 mammalian cells and performed the *in vitro* phosphatase assay on beads, with a loss-of-
216 function mutant serving as a negative control and could easily detect robust phosphatase
217 activity. This suggests that modifications or binding partners conferred in mammalian cells
218 are essential for TMEM55A phosphatase activity. Furthermore, live-cell imaging using
219 PIP2 probes also strongly indicates the *in situ* function of TMEM55A which is under the
220 control of redox state. Consistent with this, TMEM55A knockdown in mouse macrophage
221 cell lines leads to the accumulation of PIP2 and a decrease of PI5P [37].

222 As a dense layer underneath the plasma membrane, F-actin is dynamically remodeled
223 following intra- and extra-cellular signaling [38, 39]. Glucose-stimulated F-actin
224 reorganization is critical for insulin secretion in β -cells [8, 9], although this has been
225 challenged recently [40]. We showed previously that impaired regulation of β -cell actin
226 remodeling by atypical phosphatidyl inositol 3-OH kinases (PI3Ks) contributes to
227 dysfunction in T2D [41]. The PI3K signaling pathway also regulates insulin secretion by
228 recruiting insulin granules, modifying cAMP, and interleukin-1 signaling [42-44].
229 However, the role of phosphoinositide signaling pathways and F-actin remodeling on
230 glucagon secretion has not been explored. Here, we found that F-actin mainly acts as a
231 negative regulator of glucagon secretion, which agrees with other studies [11, 12]. Further,
232 we identified that the inhibition of RhoA acts as a downstream signaling event of PI5P.
233 This is in contrast to MEF cells where Rac1 and Cdc42, but not RhoA activity, were found
234 to be altered following PI5P treatment [20]. Currently, we lack an understanding of the
235 mechanism by which PI5P regulates RhoA. Viaud *et al.* demonstrated that PI5P physically
236 interacted with the exchange factor Tiam1, leading to the restricted Rac1 activation [20].
237 Numerous PI5P-interacting proteins were identified using yeast proteome

238 microarrays combined with flow cytometry [45]. It is possible that some adapter proteins
239 are involved in PI5P's action on RhoA, which requires additional study.

240 We previously demonstrated that glucose suppresses human and mouse α -cell
241 exocytosis, while non-metabolizable glucose analog 2-DG does not, due to the acute
242 glucose treatment suppressing P/Q Ca^{2+} channel activity via complex I-dependent
243 production of reactive oxygen species/ H_2O_2 [15]. However, glucose could also increase α -
244 cell exocytosis because of different culture conditions and the missing islet paracrine
245 signaling [15, 46]. Even a U-shaped response of isolated human α -cells to glucose was
246 reported [47], indicating a potential dual effect of oxidative signaling on glucagon secretion.
247 H_2O_2 was reported to increase intracellular PI5P levels in human osteosarcoma cells,
248 independently of mTOR, PDK1, PKB, ERK, p38 or PIKfyve signaling [22]. Here we found
249 that H_2O_2 could also increase PI5P (indirectly monitored as a reduction in PIP2) in α -cells
250 by activating TMEM55A. Considering in Hela cells that the type I phosphatidylinositol
251 phosphate 5-kinase (PIP5Kbeta) is involved in the response to H_2O_2 [24], it is possible that
252 diverse PIP2 kinases and phosphatases are critical in α -cell function.

253 Our correlational studies showed that α -cells with high *PIP4P2* expression in T2D
254 demonstrate lower exocytosis. Moreover, knocking down *PIP4P2* in α -cells from T2D
255 donors shows an unexpectedly higher exocytosis (Fig. S3A), suggesting that besides
256 RhoA-dependent F-actin depolymerization, PI5P might have additional roles in T2D α -
257 cells. We also tried to measure the total glucagon exocytosis from mouse *PIP4P2*
258 knockdown α -cells following 14-weeks high fat diet (HFD) to mimic the T2D condition
259 and we identified that TMEM55A still acts as a positive regulator for glucagon secretion
260 under this condition (Fig. S3B), suggesting the differences between human and mouse
261 model, which has been described before [15]. Compared with cytoplasmic PI5P, nuclear
262 PI5P was also reported to regulate gene expression and apoptosis during stress response
263 [48, 49]. It's likely that a potential excessive PI5P plays a dominant role in the nucleus
264 during diabetes. In both human and mouse α -cells, our data indicates that TMEM55A
265 positively regulates glucagon secretion in the absence of diabetes.

266 In summary, our current study highlights the importance of TMEM55A in regulating α -
267 cell exocytosis and glucagon secretion. TMEM55A is activated in response to oxidative
268 stress, such as H_2O_2 , to dephosphorylate PIP2 to PI5P, which inhibits the activation of
269 RhoA. Inhibition of RhoA will depolymerize F-actin and promote glucagon exocytosis.
270 This TMEM55A/PI5P/F-actin regulation axis is critical for glucagon secretion.

271 **Methods**

272 **Plasmids**

273 The cDNA of human *PIP4P2* was prepared by PCR using the commercial TMEM55A ORF
274 clone in a pcDNA 3.1 (Genscript; SC1200) as a template. The mammalian expression
275 vector of GFP tagged human TMEM55A (GFP-TMEM55A) was generated by inserting
276 the *PIP4P2* cDNA into PEGFPC1 plasmid that was obtained from Dr. Kiyomi Nigorikawa
277 (Hiroshima University, Japan). Loss of function mutant (GFP-TMEM55A C107S) was
278 generated using Q5 High-Fidelity 2X Master Mix (New England Biolabs, NEB) and
279 verified by sequencing. Primers used are in Table S1. F-tractin-mCherry was purchased
280 from Addgene (155218). RFP-PH-PLC was provided by Dr. Todd Alexander (University
281 of Alberta, Canada).

282

283 **siRNA constructs and quantitative PCR**

284 Human and mouse TMEM55A and scrambled siRNA were purchased from Horizon
285 Discovery Ltd (Cambridge, UK; E-013808-00-0005 and E-059670-00-0005). The FAM-
286 labeled Negative Control siRNA was from Thermo Fisher Scientific (Ottawa, ON, Canada;
287 AM4620). These were transfected in dissociated mouse, human islet cells or α TC1-9 cells
288 using LipofectamineTM RNAiMAX transfection reagent (Thermo Fisher Scientific;
289 13778075) according to the manufacturer's protocol. Quantitative PCR (qPCR) was
290 performed as previously described [50], RNA from the corresponding cells was extracted
291 72 h post-transfection using TRIzol reagent (Life Technologies, Burlington, ON), and the
292 cDNA was synthesized using OneScript[®] Plus cDNA Synthesis Kit (ABM, Richmond, BC,
293 Canada). Real-time PCR was carried out on a 7900HT Fast Real-Time PCR system using
294 PowerUpTM SYBRTM Green Master Mix (Thermo Fisher Scientific; A25742). Primers used
295 is in Table S1.

296

297 **Cell culture and transfection**

298 α TC1-9 cells (a gift from Dr. Peter Light, University of Alberta, Canada) were cultured in
299 low glucose DMEM media supplemented with 10% FBS, 0.02% BSA, 15mM HEPES, 100
300 μ M non-essential amino acids, 100 U/mL penicillin/streptomycin. The cells were kept at
301 37 °C with 10% CO₂. Human Embryonic Kidney (HEK) 293 cells (a gift from Dr. Harley
302 Kurata, University of Alberta, Canada) were cultured in high glucose DMEM media
303 supplemented with 10% FBS and 1% penicillin/streptomycin. The cells were kept at 37 °C
304 with 5% CO₂. Transfection of cDNAs was performed using Lipofectamine 3000
305 (Invitrogen; L3000008) according to the manufacturer's protocol.

306

307 **Human islets**

308 Human islets were from our Alberta Diabetes Institute IsletCore (www.isletcore.ca) [51],
309 the Clinical Islet Transplant Program at the University of Alberta, or the Human Pancreas
310 Analysis Program [52]. Human islets were cultured in DMEM media supplemented with
311 10 % FBS and 1% penicillin/streptomycin. The islets were kept at 37 °C with 5% CO₂.
312 This work was approved by the Human Research Ethics Board at the University of Alberta
313 (Pro00013094; Pro00001754) and all families of organ donors provided written informed
314 consent.

315

316 **Mouse islets**

317 Mouse islets were isolated from male C57BL/6NCrl mice (Charles River Laboratories) fed
318 with standard chow diet at 10-12 weeks of age. Mouse islets were cultured in RPMI-1640
319 with 11.1 mM glucose, 10 % FBS, 1% penicillin/streptomycin. The present mouse islet
320 study was approved by the Animal Care and use Committee at the University of Alberta
321 (AUP00000291).

322

323 **Patch-clamp recordings**

324 Patch-clamp recordings were performed as described previously [15]. Hand-picked islets
325 were dissociated into single cells using enzyme-free cell dissociation buffer (Gibco,
326 13150016) and cultured at 37°C with 5% CO₂ for 1-3 days. For depolarization-stimulated
327 exocytosis and voltage-gated Na⁺ and Ca²⁺ current measurements, media was changed to
328 a bath solution containing (in mM): 118 NaCl, 20 Tetraethylammonium-Cl, 5.6 KCl, 1.2
329 MgCl₂, 2.6 CaCl₂, 5 HEPES, and 1 glucose (pH 7.4 with NaOH) in a heated chamber
330 (37 °C). The recording pipettes with a resistance of 4-7 MΩ were fire polished, coated with
331 Sylgard and filled with the following intracellular solution (in mM): 125 Cs glutamate, 10
332 CsCl, 10 NaCl, 1 MgCl₂, 0.05 EGTA, 5 HEPES, 0.1 cAMP, and 3 MgATP (pH 7.15 with
333 CsOH). For assessment of Ca²⁺ channel activity using Ba²⁺ as a charge carrier, the bath
334 solution was composed of (in mM): 100 NaCl, 20 BaCl₂, 5 CsCl, 1 MgCl₂, 10 HEPES,
335 with 0.2 μM tetrodotoxin, 1 glucose (pH 7.4 with NaOH); and the intracellular solution
336 was composed of (in mM): 140 Cs-glutamate, 1 MgCl₂, 20 TEA, 5 EGTA, 20 HEPES, 3
337 Mg-ATP (pH 7.15 with CsOH). Electrophysiological data were recorded using a HEKA
338 EPC10 amplifier and PatchMaster Software (HEKA Instruments Inc, Lambrecht/Pfalz,
339 Germany) within 5 min of break-in. Patched cells were marked on the dish and subjected
340 to immunostaining for insulin and glucagon for cell type identification.

341

342 **In beads phosphatase assay**

343 HEK 293 cells were transfected with either GFP vector or GFP tagged-TMEM55A WT or
344 C107S mutant using Lipofectamine 3000 (Invitrogen) according to the manufacturer's
345 protocol. Those cells were solubilized in ice-cold CellLytic-M lysis buffer (Sigma-Aldrich;
346 C2978) supplemented with protease inhibitor cocktail (Sigma-Aldrich; 539137).
347 Supernatants were collected after centrifugation at 13,200 rpm for 15 min, followed by
348 incubation with GFP-Trap Agarose (Chromotek) at 4 °C. The mixture was incubated at
349 4 °C for 1 h with rotation end-over-end. Agarose beads were then washed three times using
350 washing buffer (in mM): 10 Tris-Cl pH 7.5, 150 NaCl, 0.5 EDTA, and 0.05 % NP40
351 substitute. Bead complexes were resuspended with 50 μL reaction buffer (in mM): 25 Tris-
352 Cl pH 7.4, 140 NaCl, 2.7 KCl, with or without adding 1 mM DTT or H₂O₂. Commercially
353 purchased purified SHIP2 (Cedarlane) was mixed with the reaction buffer as a positive
354 control. The reactions were processed immediately by adding diC₈-PtdIns-4,5-P₂ (PIP2)
355 (Echelon Biosciences) at a final concentration of 1 mM with incubation at 37 °C for 1 h.
356 Supernatants were collected after centrifugation at 3,000 rpm for 15 min. 100 μL Malachite
357 Green Solution (Echelon Biosciences) was mixed with 25 μL sample or phosphate standard
358 solution (0-2000 pM) in a well of the 96-well polystyrene microplate. After 20 mins
359 incubation at room temperature, absorbance was read at 620 nm. The standard curve was
360 prepared for every repeated experiment.

361

362 **GTPase activation assay**

363 The activity of Rac1/Cdc42/RhoA was measured by RhoA/Rac1/Cdc42 Activation Assay
364 Combo Biochem Kit (Cytoskeleton Inc, BK030) following a modified manufacturer
365 protocol. Briefly, islets or α TC1-9 cells were lysed in ice-cold lysis buffer (in mM): 50 Tris
366 pH 7.5, 10 MgCl₂, 500 NaCl, and 2% igepal supplemented with protease inhibitor cocktail
367 (Sigma-Aldrich). Supernatants were collected after centrifugation at 13,200 rpm for 15 min,
368 followed by incubation with rhotekin-RBD (for RhoA activation assay) or PAK-PBD beads
369 (for Rac1 and Cdc42 activation assays) at 4 °C overnight. Beads were pelleted by
370 centrifugation at 3000 rpm at 4 °C for 1 min. Beads were then washed three times using
371 washing buffer (in mM): 25 Tris pH 7.5, 30 MgCl₂, 40 NaCl and eluted by SDS loading
372 buffer. Precipitated active forms of GTPases were subjected to western blot analysis.

373

374 **Immunofluorescence**

375 Cells on the coverslips or islets were washed with PBS and fixed in 4% paraformaldehyde
376 for 15 min at room temperature, then permeabilized with 0.1% Triton X-100 for 10 min.
377 After permeabilization, cells or islets were blocked in PBS plus 3% BSA for 30 min at
378 room temperature and then incubated overnight with indicated primary antibodies in the
379 cold room, followed by incubation with corresponding secondary antibodies or together
380 with Phalloidin-iFluor 647 Reagents (Abcam, Cambridge, UK) for 1 h at room temperature.
381 Cells or islets were then mounted on the glass slides and examined using Leica TCS SP5
382 confocal laser scanning microscope (Cell Imaging Facility, Faculty of Medicine and
383 Dentistry, University of Alberta).

384

385 **Live cell imaging**

386 α TC1-9 cells were seeded into the Cellvis 35 mm glass bottom dish with 14 mm micro-
387 well #1.5 gridded (interior) cover glass (Thermo Fisher Scientific) and transfected with F-
388 tractin-mCherry or GFP-PH-PLC to visualize F-actin and PIP2, respectively. Cells were
389 pre-incubated with DMEM without any supplements 24 h before imaging. Dynamic
390 signaling following the stimulation was captured and recorded every 10 or 20 s for 10 or
391 15 min using Leica Stellaris 8 confocal microscope equipped with a live-cell chamber (Cell
392 Imaging Facility, Faculty of Medicine and Dentistry, University of Alberta). The
393 fluorescence signal intensity of F-actin or PIP2 was quantified by ImageJ.

394

395 **Glucagon secretion**

396 For static glucagon secretion measured with dispersed human islets, 50 siRNA transfected
397 islets per group were pre-incubated for 30 min in KRB buffer containing (in mM): 140
398 NaCl, 3.6 KCl, 2.6 CaCl₂, 0.5 NaH₂PO₄, 0.5 MgSO₄, 5 HEPES, 2 NaHCO₃ and 0.5 mg/ml
399 BSA supplied with 5 mM glucose. Then they were stimulated with or without glucose (1
400 mM), GIP (100 nM) and the amino acid alanine (10 mM), or KCl (20 mM). For static
401 glucagon secretion measured with α TC1-9 cells, cells plated on 12-well plates were serum
402 starved with DMEM without any supplements the day before the secretion assay. Cells
403 were washed twice with PBS and then incubated with fresh DMEM for 1 h. KCl (55 mM)
404 was used to stimulate the glucagon secretion. For some experiments, PI5P was added to
405 the fresh DMEM for 1 h incubation. For dynamic glucagon responses, 30 islets from each
406 group were pre-incubated for 30 min in KRB buffer containing (in mM): 140 NaCl, 3.6

407 KCl, 2.6 CaCl₂, 0.5 NaH₂PO₄, 0.5 MgSO₄, 5 HEPES, 2 NaHCO₃ and 0.5 mg/ml essentially
408 fatty acid free BSA. And then they were perfused in the same buffer with the changes of
409 indicated glucose concentration and the addition of GIP (100 nM) and the amino acid
410 alanine (10 mM). Total glucagon content was obtained by lysing the cells with acid ethanol
411 supplemented with protease inhibitor cocktail. All the samples were collected and stored
412 at -20 °C for assay of glucagon with either Lumit Glucagon kit (Promega; W8020) or
413 glucagon ELISA kit (MSD; K1515YK-2).

414

415 **Correlation analysis of *TMEM55A* expression against electrophysiology in patch-seq**
416 **data**

417 Raw sequencing reads are available at the NCBI Gene Expression Omnibus under the
418 following accession numbers: GSE270484, GSE124742 and GSE164875, and further
419 available at www.humanislets.com with associated electrophysiology and donor
420 characteristic. Correlations were performed using Log₂[CPM+1] values for *PIP4P2*
421 expression. Electrophysiology was corrected for outliers by only including values with a
422 z-score between 3 and -3 for each respective correlation. For total, early, and late
423 capacitance, negative values were considered noise and set to 0 to reduce their effects on
424 correlations, as they are irrelevant in contributing to functional responses for exocytosis
425 [53]. Data import, correlations with statistics, and export were performed in Python (v
426 3.7.11) using numpy (v 1.21.6), pandas (v 1.3.2), and (scipy 1.7.3) packages.

427 **Figure Legend**

428 **Figure 1. TMEM55A and islet cell function.** **A.** Representative immunofluorescence
429 images confirm TMEM55A expression in α - and β -cells of donors with no diabetes (ND)
430 or type 2 diabetes (T2D). Scale bar, 50 μ m. (n = 10 islets from 3 ND donors and 9 islets
431 from 3 T2D donors) **B-C.** Correlation of *PIP4P2* transcript expression (encodes
432 TMEM55A protein) with electrophysiological properties in human α -cells (B; n = 1114
433 cells from 45 donors) and β -cells (C; n = 229 cells from 37 donors). **D-E.** Correlation of
434 *PIP4P2* transcript expression with electrophysiological properties in human α -cells at 1
435 mM glucose (D; n = 393 cells from 33 ND donors and 75 cells from 7 T2D donors) or 5
436 mM glucose (E; n = 524 cells from 43 ND donors and 211 cells from 11 T2D donors) from
437 ND (light blue) or T2D (dark blue) donors. Data in panels B-E are from
438 www.humanislets.com. * P < 0.05; ** P < 0.01; *** P < 0.001.

439 **Figure 2. Knockdown of *PIP4P2* decreases α -cell exocytosis.** **A.** qPCR analysis of
440 *PIP4P2* mRNA expression from control (si-scramble) and *PIP4P2* knockdown (si-*PIP4P2*)
441 human islet cells (n = 3 donors). **B.** Left panel: representative western blot of TMEM55A
442 from control and *PIP4P2* knockdown human islet cells; Right panel: averaged blot
443 intensities normalized to β -actin (n = 3 donors). **C.** Left panel: representative
444 immunofluorescence images showing the TMEM55A from control and *PIP4P2*
445 knockdown human α -cells. Scale bar, 5 μ m. Positive glucagon staining is used to confirm
446 the α -cell identity. Right panel: averaged intensities per cell (n = 15 and 14 cells from 3
447 donors). **D.** Representative capacitance and current traces induced by a train of 10
448 depolarizations from -70 mV to 0 mV (gray trace) from control and *PIP4P2* knockdown
449 human α -cells. **E.** Averaged cell size (n = 28 and 29), early exocytosis (n = 28 and 29), late
450 exocytosis (n = 28 and 29), total exocytosis (n = 28 and 29), Ca^{2+} integral (n = 12 and 10)
451 and normalized exocytosis to Ca^{2+} (n = 12 and 10), calculated as total exocytosis
452 normalized to Ca^{2+} integral obtained from **D** (n = 5 donors). **F.** Left panel: glucagon
453 secretion from dispersed control and *PIP4P2* knockdown human islets at basal (5 mM
454 glucose) and stimulated conditions. Right panel: total glucagon content from left (n = 3
455 donors). **G.** Representative current traces induced by a depolymerization from -70 mV to -
456 10 mV (gray trace). **H.** Averaged Na^+ currents (n = 22 and 25), early Ca^{2+} currents (n = 24
457 and 22) and late Ca^{2+} currents (n = 24 and 22) from **G** (n = 5 donors). **I.** Left panel:
458 representative current traces obtained using a voltage jump protocol (gray trace) from
459 control and *PIP4P2* knockdown human α -cells. Right panel: averaged and normalized I-V
460 curves obtained from left panel (n = 13 and 11 cells, from 3 donors). **J.** Upper panel:
461 representative capacitance traces following 200 nM free Ca^{2+} infusion from control and
462 *PIP4P2* knockdown human α -cells. Lower panel: averaged and normalized capacitance
463 increase (ΔC_m) after 200 s infusion obtained from left panel (n = 10 and 9 cells, from 3
464 donors). Data are presented as mean \pm SD. Student's t test (panels A-C, E, H, J), or one-
465 way ANOVA and Holm-Sidak post-test (panel F). * P < 0.05; ** P < 0.01; *** P < 0.001;
466 ns – not significant.

467 **Figure 3. The effect of PIP2 and PI5P on glucagon secretion.** **A.** Averaged total
468 exocytosis with or without the infusion of 1 μ M PIP2 in human α -cells (n = 23 and 18 cells,
469 from 4 donors). **B.** Averaged total exocytosis with or without the infusion of 1 μ M PI5P in
470 human α -cells (n = 13 and 11 cells, from 3 donors). **C.** Averaged total exocytosis from
471 control, *PIP4P2* knockdown, and *PIP4P2* knockdown with PI5P infusion human α -cells.
472 (n = 11, 13 and 11 cells, from 3 donors). **D.** Averaged total exocytosis from control and
473 *PIP4P2* knockdown mouse α -cells (n = 16 and 10 cells, from 3 mice). **E.** Averaged total
474 exocytosis from control, *PIP4P2* knockdown, and *PIP4P2* knockdown with PI5P infusion
475 mouse α -cells (n = 9, 10 and 9 cells, from 3 mice). **F.** Left panel: glucagon secretion induced
476 by 2.8 mM glucose, GIP and Alaine from control mouse islets and islets with PIP2 or PI5P
477 treatments. Right panel: AUC (area under the curve) obtained from left panel (n = 6 mice).
478 **G.** Total glucagon content from F. Data are presented as mean \pm SD. Student's t test (panels
479 A, B, D), Two-way ANOVA test with mixed-effects analysis (panel F) or one-way ANOVA
480 followed by Holm-Sidak post-test (panels C, E, G). * P < 0.05; ** P < 0.01; ns – not
481 significant.

482 **Figure 4. TMEM55A regulating glucagon secretion requires its phosphatase domain.**
483 **A.** Averaged phosphatase activity from GFP, GFP-TMEM55A, GFP-TMEM55A C107S
484 and SHIP2 (n = 3). **B.** Averaged phosphatase activity of GFP-TMEM55A with the
485 treatment of DTT, H₂O₂ or DTT and H₂O₂ (n = 4). **C.** Left panel: representative images of
486 α TC1-9 cells transfected with RFP-PH-PLC (red) and GFP (green), GFP-TMEM55A, or
487 GFP-TMEM55A C107 at the basal level and after treatment with H₂O₂ (1 mM) for 15 min.
488 Scale bar, 10 μ m. Right panel: quantification of the dynamic change of the PIP2 signal
489 intensity in the α TC1-9 cells upon H₂O₂ stimulation from left (n = 8, 10 and 10 cells, from
490 3 independent experiments). **D.** Static glucagon secretion stimulated by KCl (55 mM) from
491 α TC1-9 cells transfected with si-scramble + GFP, si-*PIP4P2* + GFP, si-*PIP4P2* + GFP-
492 TMEM55A, si-*PIP4P2* + GFP-TMEM55A C107S (n = 3). **E.** Static glucagon secretion
493 stimulated by KCl (55 mM) from α TC1-9 cells with or without the treatment of PI5P (n =
494 4). Data are presented as mean \pm SD. Two-way ANOVA test with mixed-effects analysis
495 (panel C) or one-way ANOVA followed by Holm-Sidak post-test (panels A, B, D, E). * P
496 < 0.05; ** P < 0.01; *** P < 0.001; ns – not significant.

497 **Figure 5. PI5P and TMEM55A inactivate RhoA, while have no effects on Rac1 and**
498 **Cdc42.** **A.** Left panel: pull-down assays showing the levels of active forms of Rac1, Cdc42
499 and RhoA in α TC1-9 cells treated with or without PI5P (10 μ M) for 1 h. Right panel:
500 averaged and normalized active form of GTPases from left (N = 4, 3, 3). **B.** Left panel:
501 pull-down assays showing the levels of active form of Rac1, Cdc42 and RhoA for human
502 islets treated with or without PI5P (1 μ M) overnight. Right panel: averaged and normalized
503 active form of GTPases from left (n = 3, 3, 3) **C.** Left panel: pull-down assays showing the
504 levels of active form of Rac1, Cdc42 and RhoA for GFP, GFP-TMEM55A or GFP-
505 TMEM55A C107S transfected α TC1-9 cells treated with or without PI5P (10 μ M) for 1 h.
506 Right panel: averaged and normalized active form of GTPases from left (n = 3, 3, 3). Data

507 are presented as mean \pm SD. Student's test (panels A, B) or one-way ANOVA followed by
508 Holm-Sidak post-test (panels C). * $P < 0.05$; ** $P < 0.01$; *** $P < 0.001$.

509 **Figure 6. F-actin depolymerization is involved in TMEM55A's regulation on glucagon**
510 **secretion. A.** Averaged total exocytosis with or without the incubation of 10 μ M latrunculin
511 B or jasplakinolide for 1 h in human α -cells (n = 12, 11 and 9, from 3 donors). **B, C and F.**
512 Left panel: representative immunofluorescence images of human (B) and mouse (C) α -
513 cells and α TC1-9 cells (F) with or without PI5P treatment for 1 h. F-actin was visualized
514 by staining with AlexaFluor 647-phalloidin. Positive glucagon staining is used to confirm
515 the α -cell identify from dispersed human or mouse islets. Scale bar, 5 μ m. Right panel: F-
516 actin fluorescence intensity line profile analysis from left and averaged F-actin intensity
517 per cell (n = 96 and 85 cells, from 5 donors; n = 32 and 32 cells, from 3 mice; n = 34 and
518 34 cells, from 3 independent experiments). **D, E.** Representative immunofluorescence
519 images of human (D) and mouse (E) whole islets with or without PI5P treatment overnight
520 from three independent experiments. Yellow arrows indicate the disruption of F-actin.
521 Scale bar, 50 μ m **G.** Left panel: representative images of α TC1-9 cells transfected F-tractin-
522 mCherry at the basal level and after treatment with PI5P (10 μ M) for 10 min. Scale bar, 10
523 μ m. Right panel: quantification of the dynamic change of the F-actin signal intensity in the
524 α TC1-9 cells upon PI5P treatment from left (n = 6 and 7 cells, from 3 independent
525 experiments). **H.** Representative immunofluorescence images of α TC1-9 cells transfected
526 with GFP, GFP-TMEM55A or GFP-TMEM55A C107S from three independent
527 experiments. Yellow arrows indicate the disruption of F-actin. Scale bar, 10 μ m **I.** Left
528 panel: representative immunofluorescence images showing the F-actin level from control
529 and *PIP4P2* knockdown human α -cells. F-actin was visualized by staining with AlexaFluor
530 647-phalloidin. Positive glucagon staining is used to confirm the α -cell identity. Scale bar,
531 5 μ m. Right panel: F-actin fluorescence intensity line profile analysis from left and
532 averaged F-actin intensity per cell (n = 33 and 34 cells, from 3 donors). Data are presented
533 as mean \pm SD. Student's t test (panels B, C, F, I), one-way ANOVA followed by Dunnett's
534 T3 multiple comparison test (panel A), or two-way ANOVA test with mixed-effects
535 analysis (panel G). * $P < 0.05$; ** $P < 0.01$; *** $P < 0.001$.

536 **Figure 7. Schematic model showing how TMEM55A regulates glucagon secretion.** In
537 this model, upstream oxidative signals, such as H_2O_2 , activates TMEM55A. TMEM55A
538 positively regulates glucagon secretion by dephosphorylating PIP2 to PI5P and induces
539 RhoA dependent F-actin depolymerization in pancreatic α -cells.

540 **Author contributions**

541 Conceptualization, X.L. and P.E.M.; Investigation, X.L., T.dS., A.F.S., S.D., N.S., K.S.;
542 Supervision, P.E.M.; Writing, X.L., P.E.M.

543 **Declaration of Interests**

544 The authors declare no competing interests.

545 **Acknowledgements**

546 The University of Alberta is situated on Treaty 6 territory, the traditional land of First
547 Nations and Métis people. We thank Give Live Alberta and Trillium Gift of Life Network
548 (TGLN) for their work in procuring human donor pancreas for research. We also thank
549 James Lyon and Nancy Smith (Alberta) for their efforts in human islet isolation, and Kiera
550 Smith (Alberta) from Cell Imaging Core - Katz Group Centre for her assistance on live-
551 cell imaging experiments. We especially thank the organ donors and their families for their
552 kind gift supporting diabetes research.

553 This work was supported by a Foundation Grant (FS 148451) and Project Grant (PS
554 186226) to PEM from the Canadian Institutes of Health Research. We also acknowledge
555 the Human Pancreas Analysis Program (HPAP-RRID:SCR_016202)
556 (<https://hpap.pmacs.upenn.edu>), a Human Islet Research Network (RRID:SCR_014393)
557 consortium (UC4-DK-112217, U01-DK-123594, UC4-DK-112232, and U01-DK-123716).
558 This work includes data and/or analyses from HumanIslets.com funded by the Canadian
559 Institutes of Health Research, JDRF Canada, and Diabetes Canada (5-SRA-2021-1149-S-
560 B/TG 179092). XL was supported in part by fellowships from the Canadian Islet Research
561 and Training Network NSERC-CREATE program and from Alberta Innovates – Health
562 Solutions. PEM holds the Tier 1 Canada Research Chair in Islet Biology.

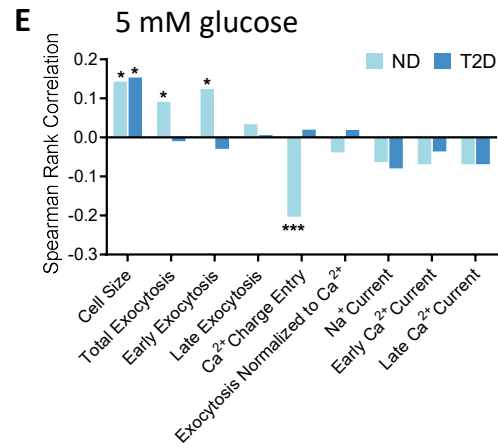
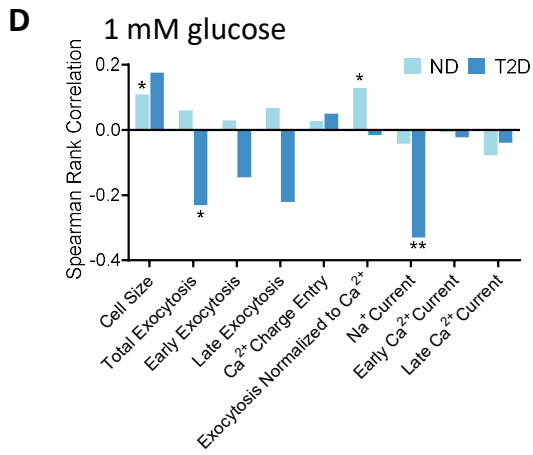
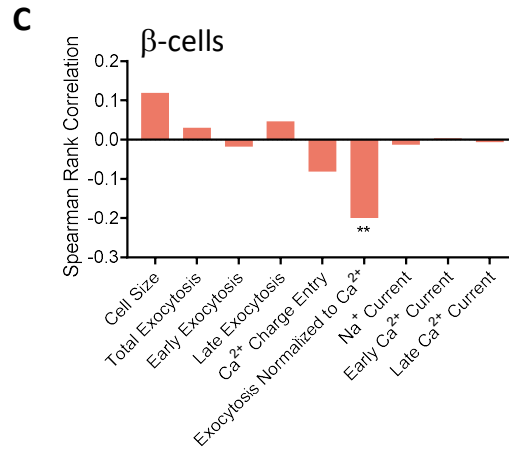
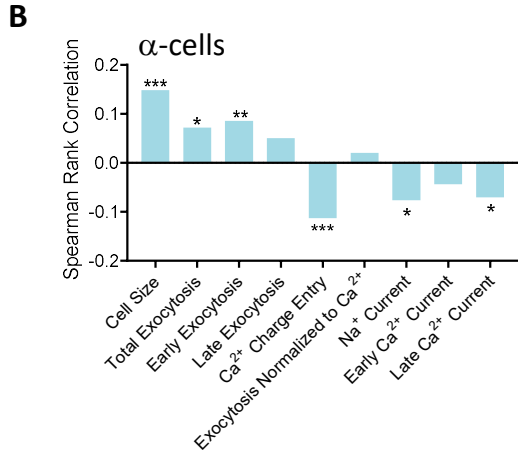
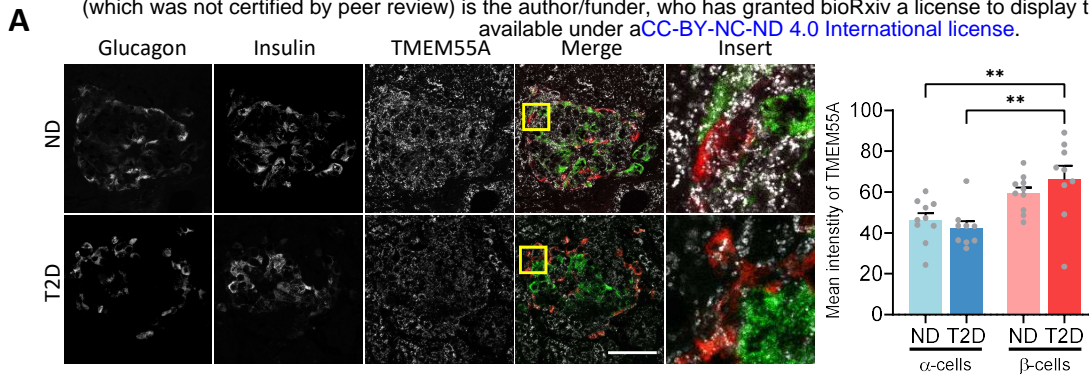
563 References

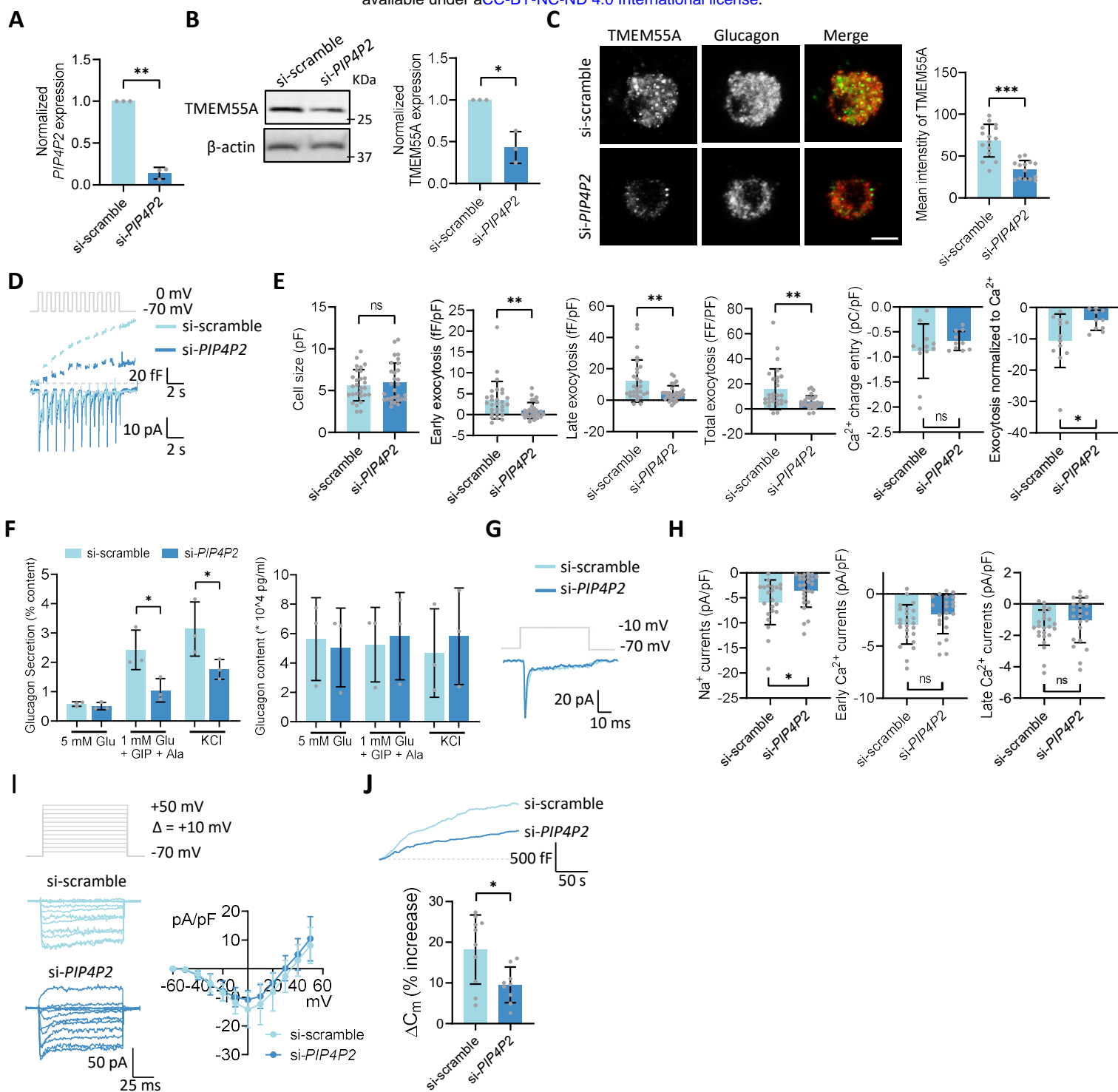
- 564 1. MacDonald, P.E. and P. Rorsman, *Metabolic Messengers: glucagon*. Nat Metab,
565 2023. **5**(2): p. 186-192.
- 566 2. Gylfe, E., *Glucose control of glucagon secretion-'There's a brand-new gimmick*
567 *every year'*. Ups J Med Sci, 2016. **121**(2): p. 120-32.
- 568 3. Bansal, P. and Q. Wang, *Insulin as a physiological modulator of glucagon secretion*.
569 Am J Physiol Endocrinol Metab, 2008. **295**(4): p. E751-61.
- 570 4. Vergari, E., et al., *Insulin inhibits glucagon release by SGLT2-induced stimulation*
571 *of somatostatin secretion*. Nat Commun, 2019. **10**(1): p. 139.
- 572 5. Gromada, J., et al., *Adrenaline stimulates glucagon secretion in pancreatic A-cells*
573 *by increasing the Ca²⁺ current and the number of granules close to the L-type*
574 *Ca²⁺ channels*. J Gen Physiol, 1997. **110**(3): p. 217-28.
- 575 6. El, K. and J.E. Campbell, *The role of GIP in O_±-cells and glucagon secretion*.
576 Peptides, 2020. **125**: p. 170213.
- 577 7. Li, P., et al., *Actin Remodeling in Regulated Exocytosis: Toward a Mesoscopic View*.
578 Trends Cell Biol, 2018. **28**(9): p. 685-697.
- 579 8. Wang, B., et al., *The adaptor protein APPL2 controls glucose-stimulated insulin*
580 *secretion via F-actin remodeling in pancreatic OI-cells*. Proc Natl Acad Sci U S A,
581 2020. **117**(45): p. 28307-28315.
- 582 9. Li, W., et al., *In situ structure of actin remodeling during glucose-stimulated insulin*
583 *secretion using cryo-electron tomography*. Nat Commun, 2024. **15**(1): p. 1311.
- 584 10. Varadi, A., T. Tsuboi, and G.A. Rutter, *Myosin Va transports dense core secretory*
585 *vesicles in pancreatic MIN6 beta-cells*. Mol Biol Cell, 2005. **16**(6): p. 2670-80.
- 586 11. Vilorio, K., et al., *Vitamin-D-Binding Protein Contributes to the Maintenance of O_±*
587 *Cell Function and Glucagon Secretion*. Cell Rep, 2020. **31**(11): p. 107761.
- 588 12. Ng, X.W., et al., *RhoA as a Signaling Hub Controlling Glucagon Secretion From*
589 *Pancreatic O_±-Cells*. Diabetes, 2022. **71**(11): p. 2384-2394.
- 590 13. Asadi, F., et al., *An orally available compound suppresses glucagon hypersecretion*
591 *and normalizes hyperglycemia in type 1 diabetes*. JCI Insight, 2024. **9**(2).
- 592 14. Ungewickell, A., et al., *The identification and characterization of two*
593 *phosphatidylinositol-4,5-bisphosphate 4-phosphatases*. Proc Natl Acad Sci U S A,
594 2005. **102**(52): p. 18854-9.
- 595 15. Dai, X.Q., et al., *Heterogenous impairment of O_± cell function in type 2 diabetes is*
596 *linked to cell maturation state*. Cell Metab, 2022. **34**(2): p. 256-268.e5.
- 597 16. Ewald, J.D., et al., *HumanIslets.com: Improving accessibility, integration, and*
598 *usability of human research islet data*. Cell Metab, 2024.
- 599 17. Omar-Hmeadi, M., A. GuđKek, and S. Barg, *Local PI(4,5)P(2) signaling inhibits*
600 *fusion pore expansion during exocytosis*. Cell Rep, 2023. **42**(2): p. 112036.
- 601 18. Walter, A.M., et al., *Phosphatidylinositol 4,5-bisphosphate optical uncaging*
602 *potentiates exocytosis*. Elife, 2017. **6**.
- 603 19. Vicinanza, M., et al., *PI(5)P regulates autophagosome biogenesis*. Mol Cell, 2015.
604 **57**(2): p. 219-34.
- 605 20. Viaud, J., et al., *Phosphatidylinositol 5-phosphate regulates invasion through*
606 *binding and activation of Tiam1*. Nat Commun, 2014. **5**: p. 4080.
- 607 21. Willett, R., et al., *TFEB regulates lysosomal positioning by modulating TMEM55B*
608 *expression and JIP4 recruitment to lysosomes*. Nat Commun, 2017. **8**(1): p. 1580.

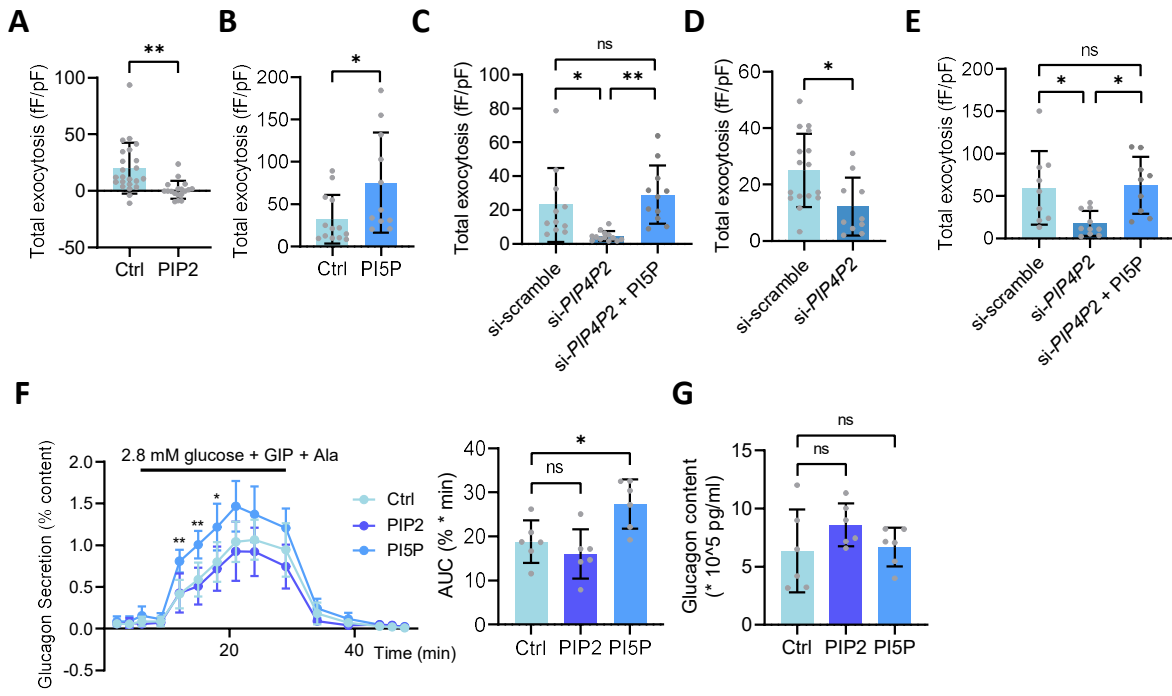
- 609 22. Jones, D.R., et al., *PtdIns5P is an oxidative stress-induced second messenger that*
610 *regulates PKB activation*. *FASEB J*, 2013. **27**(4): p. 1644-56.
- 611 23. Al-Momany, A., et al., *Clustered PI(4,5)P(2) accumulation and ezrin*
612 *phosphorylation in response to CLIC5A*. *J Cell Sci*, 2014. **127**(Pt 24): p. 5164-78.
- 613 24. Chen, M.Z., et al., *Oxidative stress decreases phosphatidylinositol 4,5-*
614 *bisphosphate levels by deactivating phosphatidylinositol- 4-phosphate 5-kinase*
615 *beta in a Syk-dependent manner*. *J Biol Chem*, 2009. **284**(35): p. 23743-53.
- 616 25. Rameh, L.E. and R.D. Blind, *25B Years of PI5P*. *Front Cell Dev Biol*, 2023. **11**: p.
617 1272911.
- 618 26. Oppelt, A., et al., *Production of phosphatidylinositol 5-phosphate via PIKfyve and*
619 *MTMR3 regulates cell migration*. *EMBO Rep*, 2013. **14**(1): p. 57-64.
- 620 27. Ramel, D., et al., *Shigella flexneri infection generates the lipid PI5P to alter*
621 *endocytosis and prevent termination of EGFR signaling*. *Sci Signal*, 2011. **4**(191):
622 p. ra61.
- 623 28. Spiering, D. and L. Hodgson, *Dynamics of the Rho-family small GTPases in actin*
624 *regulation and motility*. *Cell Adh Migr*, 2011. **5**(2): p. 170-80.
- 625 29. Bisaria, A., et al., *Membrane-proximal F-actin restricts local membrane*
626 *protrusions and directs cell migration*. *Science*, 2020. **368**(6496): p. 1205-1210.
- 627 30. Nolan, C.J., P. Damm, and M. Prentki, *Type 2 diabetes across generations: from*
628 *pathophysiology to prevention and management*. *Lancet*, 2011. **378**(9786): p. 169-
629 81.
- 630 31. Kahn, S.E., M.E. Cooper, and S. Del Prato, *Pathophysiology and treatment of type*
631 *2 diabetes: perspectives on the past, present, and future*. *Lancet*, 2014. **383**(9922):
632 p. 1068-83.
- 633 32. Scherm, M.G., et al., *Beta cell and immune cell interactions in autoimmune type 1*
634 *diabetes: How they meet and talk to each other*. *Mol Metab*, 2022. **64**: p. 101565.
- 635 33. Girard, J., *Glucagon, a key factor in the pathophysiology of type 2 diabetes*.
636 *Biochimie*, 2017. **143**: p. 33-36.
- 637 34. Pal, P., et al., *Parkinson's VPS35[D620N] mutation induces LRRK2-mediated*
638 *lysosomal association of RILPL1 and TMEM55B*. *Sci Adv*, 2023. **9**(50): p.
639 eadj1205.
- 640 35. Rudnik, S., et al., *S-palmitoylation determines TMEM55B-dependent positioning*
641 *of lysosomes*. *J Cell Sci*, 2022. **135**(5).
- 642 36. Takemasu, S., et al., *Phosphorylation of TMEM55B by Erk/MAPK regulates*
643 *lysosomal positioning*. *J Biochem*, 2019. **166**(2): p. 175-185.
- 644 37. Morioka, S., et al., *TMEM55a localizes to macrophage phagosomes to*
645 *downregulate phagocytosis*. *J Cell Sci*, 2018. **131**(5).
- 646 38. Kalwat, M.A. and D.C. Thurmond, *Signaling mechanisms of glucose-induced F-*
647 *actin remodeling in pancreatic islet OI cells*. *Exp Mol Med*, 2013. **45**(8): p. e37.
- 648 39. Eitzen, G., *Actin remodeling to facilitate membrane fusion*. *Biochim Biophys Acta*,
649 2003. **1641**(2-3): p. 175-81.
- 650 40. Polino, A.J., et al., *Disrupting actin filaments enhances glucose-stimulated insulin*
651 *secretion independent of the cortical actin cytoskeleton*. *J Biol Chem*, 2023.
652 **299**(11): p. 105334.

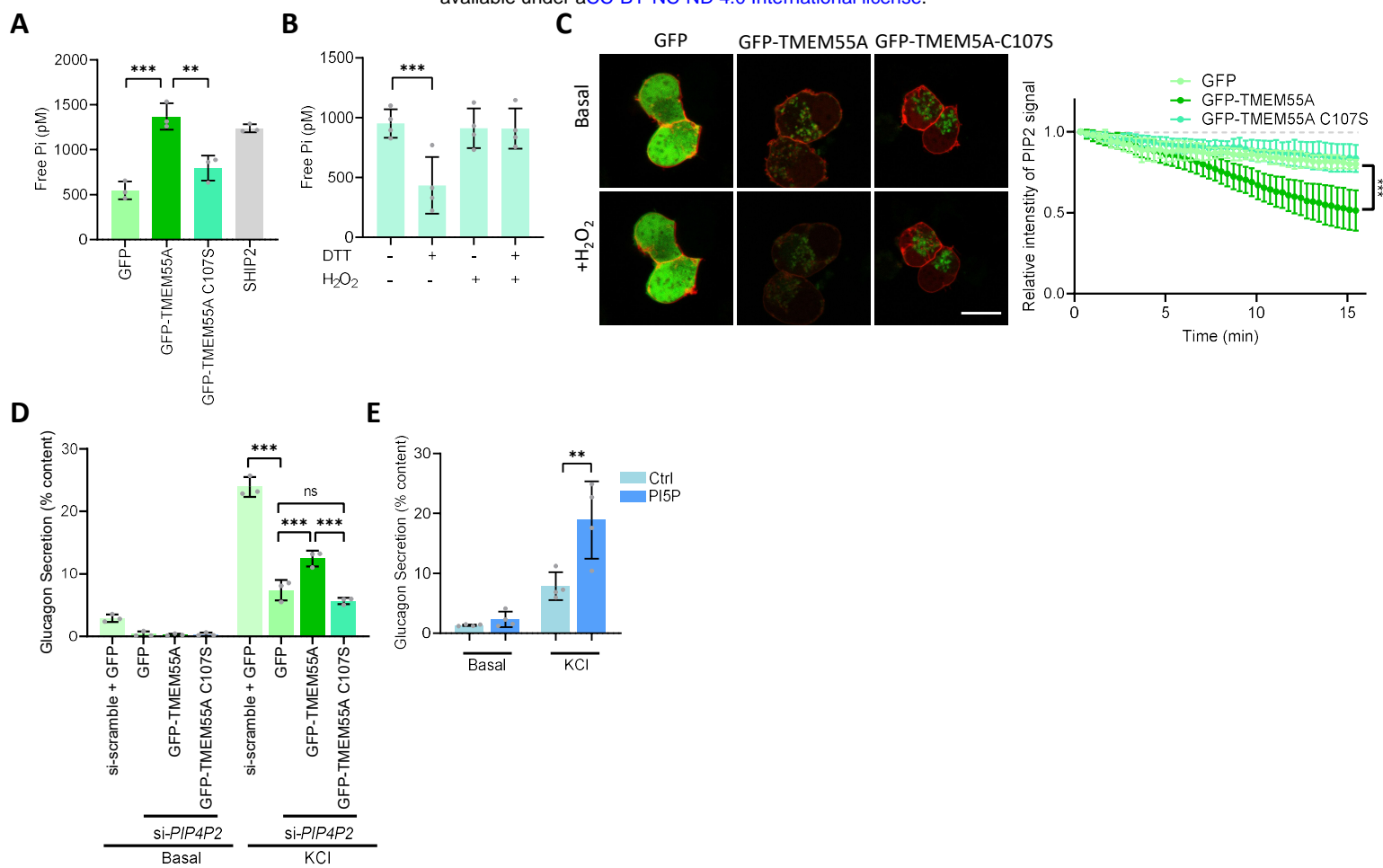
- 653 41. Kolic, J., et al., *PI3 kinases p110 α and PI3K-C2OI negatively regulate cAMP via*
654 *PDE3/8 to control insulin secretion in mouse and human islets*. Mol Metab, 2016.
655 **5**(7): p. 459-471.
- 656 42. Kolic, J., et al., *Insulin secretion induced by glucose-dependent insulintropic*
657 *polypeptide requires phosphatidylinositol 3-kinase O α in rodent and human OI-cells*.
658 J Biol Chem, 2014. **289**(46): p. 32109-32120.
- 659 43. Pigeau, G.M., et al., *Insulin granule recruitment and exocytosis is dependent on*
660 *p110 γ in insulinoma and human beta-cells*. Diabetes, 2009. **58**(9): p. 2084-
661 92.
- 662 44. Hajmrle, C., et al., *Interleukin-1 signaling contributes to acute islet compensation*.
663 JCI Insight, 2016. **1**(4): p. e86055.
- 664 45. Herianto, S., et al., *Systematic Analysis of Phosphatidylinositol-5-phosphate-*
665 *Interacting Proteins Using Yeast Proteome Microarrays*. Anal Chem, 2021. **93**(2):
666 p. 868-877.
- 667 46. Olsen, H.L., et al., *Glucose stimulates glucagon release in single rat alpha-cells by*
668 *mechanisms that mirror the stimulus-secretion coupling in beta-cells*.
669 Endocrinology, 2005. **146**(11): p. 4861-70.
- 670 47. Omar-Hmeadi, M., et al., *Paracrine control of O α -cell glucagon exocytosis is*
671 *compromised in human type-2 diabetes*. Nat Commun, 2020. **11**(1): p. 1896.
- 672 48. Gozani, O., et al., *The PHD finger of the chromatin-associated protein ING2*
673 *functions as a nuclear phosphoinositide receptor*. Cell, 2003. **114**(1): p. 99-111.
- 674 49. Shi, X., et al., *ING2 PHD domain links histone H3 lysine 4 methylation to active*
675 *gene repression*. Nature, 2006. **442**(7098): p. 96-9.
- 676 50. Lin, H., et al., *A role and mechanism for redox sensing by SENP1 in OI-cell*
677 *responses to high fat feeding*. Nat Commun, 2024. **15**(1): p. 334.
- 678 51. Lyon, J.G., et al., *Human research islet cell culture outcomes at the Alberta*
679 *Diabetes Institute IsletCore Islets*, 2024. **16**(1): p. 2385510.
- 680 52. Shapira, S.N., et al., *Understanding islet dysfunction in type 2 diabetes through*
681 *multidimensional pancreatic phenotyping: The Human Pancreas Analysis Program*.
682 Cell Metab, 2022. **34**(12): p. 1906-1913.
- 683 53. Camunas-Soler, J., et al., *Patch-Seq Links Single-Cell Transcriptomes to Human*
684 *Islet Dysfunction in Diabetes*. Cell Metab, 2020. **31**(5): p. 1017-1031 e4.

685

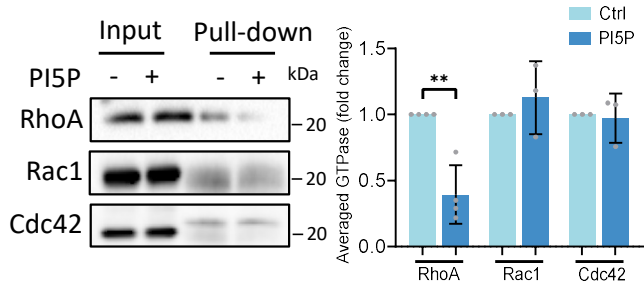




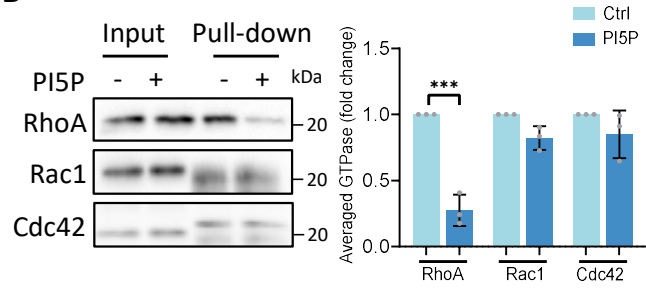




A



B



C

